[14]See, e.g., R. G. Kepler, in *Treatise on Solid State Chemistry*, edited by N. B. Hannay (Plenum, New York, 1976), Vol. 3, p. 650.
[15]N. F. Mott, E. A. Davis, and R. A. Street, Philos. Mag. 32, 961 (1975).
[16]D. Emin, private communication. See also, R. C. Hughes and D. Emin, in *Proceedings of the First Topical Conference on the Physics of SiO_2 and Its Interfaces, Yorktown Heights, New York, 1978*, edited by S. T. Pantelides (Pergamon, New York, 1978).

Resolved Structure within the Broad-Band Vibrational Raman Line of Liquid H_2O from Polarization Coherent Anti-Stokes Raman Spectroscopy

N. I. Koroteev,[a] M. Endemann, and R. L. Byer
Applied Physics Department, Stanford University, Stanford, California 94305
(Received 21 May 1979)

We have resolved individual components of the broad vibrational band of liquid water by using polarization coherent anti-Stokes (active) Raman spectroscopy. None of the existing models of liquid water based on the unresolved spontaneous Raman spectrum describe in full the observed spectra.

The unambiguous resolution of close and overlapping lines is one of the most important and difficult problems in spectroscopy. In spontaneous Raman spectroscopy of condensed substances the solution to this problem is a curve-fitting procedure involving a formal resolution of observed bands into a number of symmetrical lines of chosen shape and intensity. However, this technique suffers from the lack of uniqueness as a consequence of the lack of resolution. A well-known and important example of the lack of uniqueness is the variety of models proposed to describe the spontaneous Raman line shape of liquid water in the 3200–3600-cm^{-1} stretching-vibrational region.[1-5]

In this Letter we show that active control of the polarization in coherent anti-Stokes (active) Raman spectroscopy (CARS) offers the spectroscopist a new tool with which to probe the inner structure of broad Raman bands. We apply the technique to the 3400-cm^{-1} band of liquid water and resolve spectral details that can be used to verify existing models of this band and thus the structure of water in the liquid state.

The ability of polarization CARS to resolve components was discussed and experimentally used to resolve the doublet structure of the 1305-cm^{-1} Raman line of an aqueous solution of HNO_3.[6,7] Here we develop this technique in more detail with emphasis on broad featureless bands.

Consider a simple example of a pair of closely spaced Raman lines with Lorentzian line shapes and identical linewidths and intensities but with slightly different depolarization ratios (i.e., $\rho_1 = 0.32$ and $\rho_2 = 0.35$). Figure 1(a) shows the resulting spontaneous Raman band shape when the two components are closer than their full width at half maximum (FWHM) linewidths. The band shape becomes indistinguishable from the individual components and hence the band is unresolved. A similar unresolved band shape occurs for ordinary CARS where the frequency dispersion of $|\chi_{1111}^{(3)}(\omega_a; \omega_1, -\omega_2)|^2$ is measured as shown in Fig. 1(b).

However, polarization CARS does allow the band shape to be resolved as shown in Fig. 1(c). Here the polarization vectors $\vec{e}_1$ and $\vec{e}_2$ of the linearly polarized waves at frequencies ω_1 and ω_2 make an angle $\rho = 70°$ with respect to each

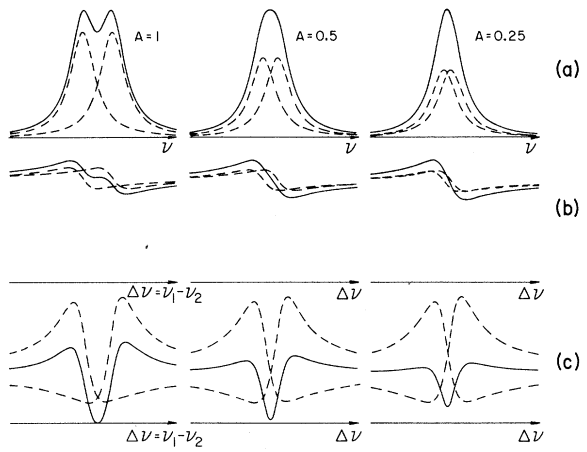

FIG. 1. Pair of overlapping lines in (a) spontaneous Raman spectroscopy, (b) ordinary CARS, and (c) polarization CARS. The parameter of curves is the relative distance between the line centers, $A = (\Omega_1 - \Omega_2)/\text{FWHM}$. In (c), the angle ϵ between $\vec{p}_{NR}$ and the normal of the analyzer transmission plane is chosen to be $\epsilon = 0.14°$; $\chi_{1111}^{(3)R1}/\chi_{1111}^{(3)NR} = 0.1$.

other. A polarization analyzer is used in the anti-Stokes beam and is set near the position to suppress the nonresonant background.[7] The three contributions to the nonlinear polarization at $\omega_a = 2\omega_1 - \omega_2$ are

$$\vec{P}^{(3)}(\omega_a) = \chi_{1111}^{(3)NR}\vec{p}_{NR} + \chi_{1111}^{(3)R1}\vec{p}_{R1} + \chi_{1111}^{(3)R2}\vec{p}_{R2}, \quad (1)$$

where

$$\vec{p}_{NR} = 2\vec{e}_1(\vec{e}_1\cdot\vec{e}_2^{\,*}) + \vec{e}_2^{\,*}(\vec{e}_1\cdot\vec{e}_1) \quad (2)$$

gives the polarization of the nonresonant background and

$$\vec{p}_{R1\,(R2)} = 3(1-\rho_{R1\,(R2)})\,\vec{e}_1(\vec{e}_1\cdot\vec{e}_2^{\,*}) + 3\rho_{R1\,(R2)}\,\vec{e}_2^{\,*}(\vec{e}_1\cdot\vec{e}_1) \quad (3)$$

determines the polarization of each of the Raman resonances. If the normal of the transmission plane of the analyzer is set between $\vec{p}_{R1}$ and $\vec{p}_{R2}$, their projections on this plane are of opposite sign thus leading to destructive interference. The interference condition can be "actively" controlled by rotation of the analyzer. Thus the closely spaced lines that compose the band can be resolved in polarization CARS even though they remain unresolved in spontaneous Raman and ordinary CARS spectroscopy.

The experimental setup for applying the polarization CARS technique to liquid water is shown in Fig. 2. The high-peak-power computer-tuned

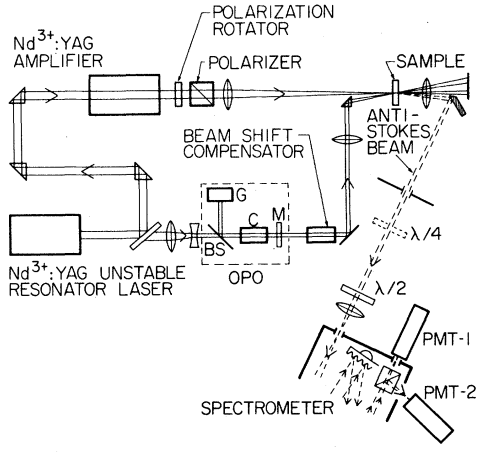

FIG. 2. Schematic of the measurement apparatus showing the unstable resonantor Nd:YAlG-laser-pumped $LiNbO_3$ OPO tunable source which consists of a 5-cm $LiNbO_3$ crystal (C), grating (G), output coupler (M), and input beam splitter (BS). $\lambda/4$ and $\lambda/2$ are Fresnel rhomb dispersionless quarter- and half-wave plates and PMT-1 and -2 are the signal and reference photomultiplier detectors.

1.4–4.0-μm Nd:YAlG-laser–pumped (neodymium-doped yttrium aluminum garnet) $LiNbo_3$ optical parametric oscillator (OPO) source easily covers the entire liquid-water Raman spectrum from 2900 to 3100 cm^{-1} by tuning over the 1.53–1.89-μm Stokes wavelength range relative to the 1.064-μm pump wavelength of the unstable resonator Nd:YAlG laser.[8] The absorption of the parametric oscillator radiation by liquid water is still moderate $l_{absorp} \simeq 0.1$ cm in this wavelength region.[9] Small anamolous dispersion of the water-refractive index prevents angle phase matching by beam crossing. However, we used slightly crossed beams to allow spatial separation of the generated anti-Stokes beam.

Typical beam powers at the sample were 3.5 MW at 1.064 μm and 0.1 MW at the Stokes wave. Both beams were focused to a diameter of 0.5 mm inside the sample. The cell was constructed with use of thin 0.2-mm glass windows to decrease anti-Stokes generation in the glass. Measurements were made at room temperature on singly distilled water. The temperature rise due to absorbed optical power was estimated to be less than 5°C. A PDP-11/10 minicomputer was used to synchronously tune the $LiNbO_3$ optical parametric oscillator[10] and the grating spectrometer.

Attention was paid to systematic changes in the anti-Stokes signal due to dispersion of the coherence length and absorption of the Stokes beam. In water, $l_{coh} = 0.6$ mm at 2900 cm^{-1} and 0.2 mm at 4100 cm^{-1} where $l_{coh} = \pi/\Delta k$. The systematic variation of the anti-Stokes signal as well as fluctuations in its intensity were normalized by rationing the signal transmitted by the analyzer to the orthogonally polarized component rejected by the analyzer thus exploiting a technique recently developed by Oudar, Smith, and Shen.[11]

The computer collected data from signal and reference channels on each laser pulse at a 10-Hz rate, calculated their ratio, averaged over 50 pulses, calculated the statistical deviation of the ratio, and stored the data on disk. Spectral scans which were run several times were taken in 15-cm^{-1} steps resulting in scan times of nearly half an hour.

For each angle position of the analyzer we took a polarization CARS spectrum with and without a quarter-wave plate in the anti-Stokes beam. This provided complete information on the change in elliptical polarization of the CARS signal[11] and gave spectra that were equivalent to the two dispersion curves, ellipticity and major-axis in-

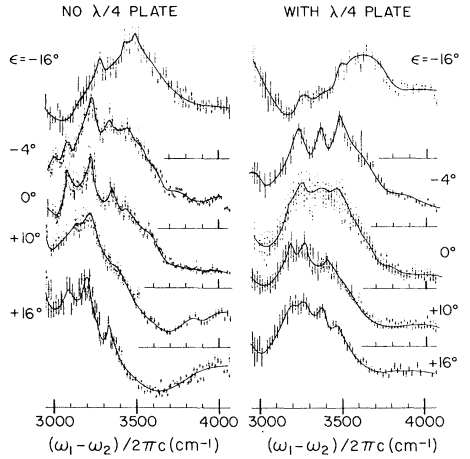

FIG. 3. Polarization CARS spectra of liquid water for various angles ϵ between $\vec{p}_{NR}$ and the normal of the analyzer transmission plane as a parameter. The spectra on the left show the dispersion of the ratio of the signal and reference photomultiplier signals. The spectra on the right show the same, but with a quarter-wave plate placed in the anti-Stokes beam with its principal axis at an angle of $-3°$ relative to $\vec{p}_{NR}$.

clination-angle dispersion, usually studied by coherent Raman ellipsometry (CREM).[7,12]

Figure 3 shows selected examples of the observed spectra at various setting angles of the analyzer. Here the analyzer angle ϵ is referred to the normal to the transmission plane and the nonresonant background polarization vector $\vec{p}_{NR}$. The measured angle between $\vec{p}_{NR}$ and $\vec{e}_1$ was $\varphi_{\text{expt}} = 46° \pm 0.5°$ compared to the calculated angle of $\varphi_{\text{calc}} = \tan^{-1}(\frac{1}{3}\tan\varphi) = 42.4°$ at $\varphi = 70°$ assuming that Kleinman's symmetry applies for $x_{ijkl}^{(3)NR}$.[12] No nonresonant background signal was observed for the analyzer angle set to $\epsilon = 0°$. In the present geometry $\epsilon > 0$ corresponds to the vector $\vec{p}_{NR}$ lying between $\vec{e}_1$ and the normal to the analyzer transmission plane.

Figure 4 shows the computer-simulated polarization CARS spectra of liquid water using the data of various proposed models. For these calculations we have taken the number of components, their positions, FWHM, integrated intensities, and depolarization ratios from models proposed by Murphy and Bernstein[3] and by Scherer and others[5] as well as an early model due to Schultz and Hornig.[1] The fitting parameter for the curves was the ratio of the peak value of the imaginary part of the resonant Raman susceptibility tensor $\chi_{1111}^{(3)R}$, to the nonresonant component $\chi_{1111}^{(3)NR}$, of water. The closest qualitative agreement of calculated and observed spectra was achieved with $\chi_{1111}^{(3)R}/\chi_{1111}^{(3)NR} \approx 0.65$, which

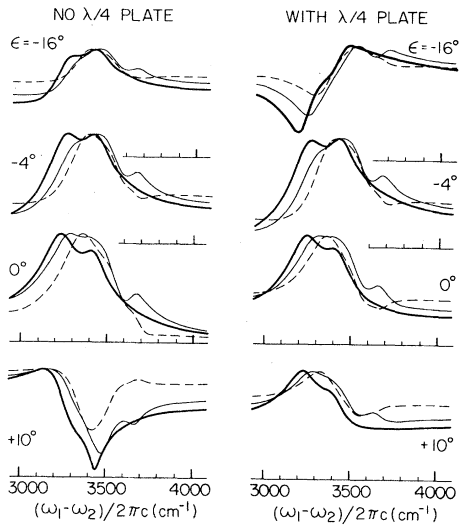

FIG. 4. Computer-simulated polarization CARS spectra of water. All conditions are equivalent to that of Fig. 3. Heavy solid lines, Murphy and Bernstein's model (Ref. 3); light solid lines, model of Scherer and others (Ref. 5); dashed lines, Schultz and Hornig's model (Ref. 1). $\chi_{1111}^{(3)R}/\chi_{1111}^{(3)NR} = 0.65$. Dispersion of l_{coh} in water was calculated using data on water refractive index. The ratio of nonresonant cubic susceptibilities of water and glass $(\chi_{1111}^{(3)NR})_{\text{glass}}/(\chi_{1111}^{(3)NR})_{\text{water}} = 0.63$ was taken from Levine and Bethea's papers[14] (see also Ref. 15, Table 14.1).

is 3 times less than reported by Itzkin and Leonard in their early CARS studies of H_2O.[13] Although the calculated spontaneous Raman spectra are nearly identical for the models, this is clearly not the case for the calculated polarization CARS spectra. The Schultz-Hornig model results in curves qualitatively inconsistent with observed spectra which appear to more closely match the experimental ones. However, there is significant quantitative disagreement between theory and experimental for all of the models considered.

In conclusion, we have shown that polarization CARS is a powerful tool for studying the structure of broad Raman bands. We have resolved, for the first time, the fine structure of the water stretching-vibrational Raman band by controlling the polarization in CARS spectroscopy. This experiment clearly demonstrates the advantages of polarization coherent anti-Stokes (active[7,12]—as it is sometimes and properly called) Raman spectroscopy.

One of us (N.K.), acknowledges fruitful discussions with S. A. Akhmanov, R. W. Hellwarth, and M. D. Levenson. This work was partially supported by the National Science Foundation and par-

tially by the International Research and Exchanges (IREX) program.

[a]On sabbatical leave from the Department of Physics, Moscow State University, Moscow 117234, U. S. S. R.

[1]J. W. Schultz and D. F. Hornig, J. Phys. Chem. 65, 2131 (1961).

[2]G. E. Walrafen, in *Water, A Comprehensive Treatise*, edited by F. Franks (Plenum, New York, 1972), Vol. 1, Chap. 5.

[3]W. F. Murphy and J. M. Bernstein, J. Phys. Chem. 76, 1147 (1972).

[4]K. Cunningham and P. A. Lyons, J. Chem. Phys. 59, 2132 (1973).

[5]J. R. Scherer, M. K. Go, and S. Kint, J. Phys. Chem. 78, 1304 (1974).

[6]A. F. Bunkin, M. G. Karimov, N. I. Koroteev, Vestn. Mosk. Univ., Ser. Fiz. Astronomiya 19, 3 (1978).

[7]S. A. Akhmanov, A. F. Bunkin, S. G. Ivanov, and N. I. Koroteev, Zh. Eksp. Teor. Fiz. 74, 1272 (1978) [Sov. Phys. JETP, 47, 667 (1978)].

[8]R. L. Herbst, H. Komine, and R. L. Byer, Opt. Commun. 21, 5 (1977).

[9]W. Luck, Fortschr. Chem. Forsch. 4, 653 (1964).

[10]R. L. Byer and R. L. Herbst, in *Topics in Applied Physics: Nonlinear Infrared Generation*, edited by Y. R. Shen (Springer, Berlin, 1977), Vol. 16, pp. 87–137.

[11]J. L. Oudar, R. W. Smith, and Y. R. Shen, to be published.

[12]S. A. Akhmanov and N. I. Koroteev, Usp. Fiz. Nauk 123, 405 (1977) [Sov. Phys. Usp. 20, 899 (1977)].

[13]I. Itzkan and D. A. Leonard, Appl. Phys. Lett. 26, 106 (1975).

[14]B. F. Levine and C. G. Bethea, J. Chem. Phys. 65, 2429 (1976); C. G. Bethea, Appl. Opt. 14, 2435 (1975).

[15]R. W. Hellwarth, in *Progress in Quantum Electronics*, edited by John Sanders (Pergamon, Oxford and New York, 1977), Vol. 5, Pt. I.

Hall-Effect Analysis of Persistent Photocurrents in *n*-GaAs Layers

H. J. Queisser and D. E. Theodorou[a]

Max-Planck-Institut für Festkörperforschung, D-7000 Stuttgart 80, Federal Republic of Germany

(Received 22 May 1979)

The buildup of persistent photoconductivity, presently a controversial phenomenon, is observed by measuring densities and mobilities of photoinduced excess electrons in thin *n*-GaAs layers between successive illuminations. Evidence from this novel type of analysis supports a model assuming charge separation by macroscopic potential barriers. We explain quantitatively how the photon dose logarithmically increases the number, but not necessarily the density, of persisting carriers and ascribe mobility enhancements to screening of ionized impurities.

Many semiconductors exhibit persistent photocurrents (PP): A photoinduced conductivity increment persists *after* the illumination, often with immeasurably long time constants.[1-7] Two conflicting interpretations presently exist. The first assumes *macroscopic* potential barriers, such as junctions or surface barriers, which separate spatially the photogenerated electron/hole pairs to suppress their recombination.[1-4] The second interpretation postulates *microscopic* barriers against recombination due to impurity atoms with large lattice relaxations.[5-7]

Interest in this unusual phenomenon has been recently rekindled. Studies of two-dimensional electron gases at semiconductor interfaces rely on PP to enhance electron densities.[8] Interpretations of atomistic properties of deep impurities in semiconductors have been based on PP observations.[6,7] Enhancement of carrier mobility by spatial separation of liberated carriers from their dopant ions ("modulation doping")[9] may be related to PP. Quantitative information is needed to describe lateral charge transport in very thin semiconductor layers near surfaces. This would be of interest for quantum effects from reduced dimensionality[10] as well as for applications, such as charge-coupled devices[11] or memories.[2]

This paper describes PP in well-defined layers of GaAs at low photon excitation levels. We are able to observe and explain for the first time the transient buildup of PP by using the Hall effect with high resolution to measure both density n and mobility μ of the excess electrons in thin n-type layers on high-resistivity substrates. This technique, which yields more information than simple conductance measurements, is shown here to furnish quantitative details about geometric structure and electronic transport. The method thus promises to become a novel technique for analysis of semiconductors interfaces. We obtain clear evidence for the model, assuming macroscopic barriers.

